Published online 25 March 2016

Nucleic Acids Research, 2016, Vol. 44, No. 13 ***6127–6141***
doi: 10.1093/nar/gkw202

Structure and function of human histone H3.Y nucleosome

Tomoya Kujirai[1], Naoki Horikoshi[2], Koichi Sato[1], Kazumitsu Maehara[3], Shinichi Machida[1], Akihisa Osakabe[1], Hiroshi Kimura[4], Yasuyuki Ohkawa[3] and Hitoshi Kurumizaka[1,2,5,*]

[1]Laboratory of Structural Biology, Graduate School of Advanced Science and Engineering, Waseda University, 2-2 Wakamatsu-cho, Shinjuku-ku, Tokyo 162-8480, Japan, [2]Research Institute for Science and Engineering, Waseda University, 2-2 Wakamatsu-cho, Shinjuku-ku, Tokyo 162-8480, Japan, [3]Division of Transcriptomics, Medical Institute of Bioregulation, Kyushu University, 3-1-1 Maidashi, Higashi-ku, Fukuoka 812-8582, Japan, [4]Department of Biological Sciences, Graduate School of Bioscience and Biotechnology, Tokyo Institute of Technology, Yokohama 226-8501, Japan and [5]Institute for Medical-oriented Structural Biology, Waseda University, 2-2 Wakamatsu-cho, Shinjuku-ku, Tokyo 162-8480, Japan

Received September 03, 2015; Revised March 16, 2016; Accepted March 16, 2016

ABSTRACT

Histone H3.Y is a primate-specific, distant H3 variant. It is evolutionarily derived from H3.3, and may function in transcription regulation. However, the mechanism by which H3.Y regulates transcription has not been elucidated. In the present study, we determined the crystal structure of the H3.Y nucleosome, and found that many H3.Y-specific residues are located on the entry/exit sites of the nucleosome. Biochemical analyses revealed that the DNA ends of the H3.Y nucleosome were more flexible than those of the H3.3 nucleosome, although the H3.Y nucleosome was stable *in vitro* and *in vivo*. Interestingly, the linker histone H1, which compacts nucleosomal DNA, appears to bind to the H3.Y nucleosome less efficiently, as compared to the H3.3 nucleosome. These characteristics of the H3.Y nucleosome are also conserved in the H3.Y/H3.3 heterotypic nucleosome, which may be the predominant form in cells. In human cells, H3.Y preferentially accumulated around transcription start sites (TSSs). Taken together, H3.Y-containing nucleosomes around transcription start sites may form relaxed chromatin that allows transcription factor access, to regulate the transcription status of specific genes.

INTRODUCTION

Histones H2A, H2B, H3 and H4 are the major protein components of chromatin, which packages the genomic DNA within the nucleus in eukaryotes (1). The basic unit of chromatin is the nucleosome, in which about 150 base pairs of DNA and a histone octamer, containing two each of H2A, H2B, H3 and H4, form a disc-like structure (2). In the nucleosome, the DNA is tightly wrapped around the histone octamer, and is generally inaccessible to DNA binding proteins. To overcome this nucleosome barrier, cells modulate the structures and dynamics of nucleosomes to regulate genomic DNA functions. The histone composition and the chromatin structure around transcription start sites (TSSs) are distinct from those of protein coding regions (gene bodies), especially in actively transcribing genes (3,4). Therefore, the specific chromatin architecture may play an essential role in transcription regulation.

Histone modifications may function to modulate chromatin structures, and to up- and down-regulate gene expression in chromatin (5,6). In addition, non-allelic isoforms of histones H2A and H3 have been widely found in eukaryotes, from yeast to mammals (7). Among the histone H3 variants, H3.3, H3T (H3.4), H3.5, H3.X, H3.Y and CENP-A (CenH3) have been identified in humans (8–19), in addition to the two canonical H3.1 and H3.2 variants, which are produced in S-phase cells (15,16,20,21). These H3 variants have different expression profiles in tissues, suggesting that they may perform specific functions during cell differentiation and tissue development (15,16,21–26).

Histone H3.Y has been identified as a primate-specific, distant H3 variant evolutionarily derived from H3.3. A previous study reported that, in humans, H3.Y is expressed in several normal and malignant tissues (18). H3.Y is also present in the human hippocampus, highlighting the possibility that H3.Y may have a specific function in brain development. Interestingly, H3.Y preferentially accumulates in euchromatin, and the H3.Y knockdown leads to more genes being transcriptionally suppressed, rather than enhanced (18). In addition, endogenous H3.Y production was observed in some osteosarcoma cells, and, intriguingly, the H3.Y production was enhanced by particular stress stimuli

*To whom correspondence should be addressed. Tel: +81 3 5369 7315; Fax: +81 3 5367 2820; Email: kurumizaka@waseda.jp

(18). The H3.Y knockdown leads to changes in the expression of genes involved in cell cycle progression, and consequently diminished cell growth (18). These lines of evidence suggest that the nucleosome containing H3.Y may play a role in transcription activation and may function in cell differentiation. However, no link between the function and structure of H3.Y has been established.

In the present study, we determined the crystal structure of the H3.Y nucleosome, and analyzed the biochemical and structural properties of the H3.Y nucleosome *in vitro*. The *in vivo* mobility and genome-wide localization of H3.Y were also studied. The results consistently suggested that H3.Y is stably assembled at TSSs, to form an accessible chromatin configuration with flexible DNA ends and reduced linker histone H1 binding.

MATERIALS AND METHODS

Purification of recombinant human histones and Nap1

The DNA fragment encoding human H3.Y was prepared by site-directed mutagenesis of the DNA fragment encoding human H3.3. The H3.Y DNA fragment was inserted into the pET15b vector, and expressed in *Escherichia coli* BL21(DE3). Purification of human histones was performed by the method described previously (27,28). For the preparation of the heterotypic nucleosome containing H3.Y and H3.3, His_6-SUMO tagged H3.3 was used, and the heterotypic nucleosome was prepared by the method described previously (29). Human Nap1 was purified as described previously (30). The DNA fragment encoding human histone H1.2 was inserted into the pET21a vector, as the C-terminally SUMO-fused protein. The H1.2-SUMO-His_6 fusion protein was produced in the *E. coli* BL21 (DE3) strain, which contains the minor tRNA expression vector (Codon(+)RIL; Stratagene), and was purified by the method described previously (31). The SUMO-His_6 portion was removed by PreScission protease. After the removal of the SUMO-His_6, six amino residues, Leu-Glu-Val-Leu-Phe-Gln, remained at the C-terminus of H1.2.

Preparation of nucleosomes

The palindromic 146 base-pair satellite DNA fragment (2) and the 193 base-pair DNA fragment containing the Widom 601 sequence (32) were purified by the methods described previously (33,34). For reconstitution of the H3.Y nucleosome, H2A, H2B, H3.Y, and H4 were mixed in 20 mM Tris-HCl buffer (pH 7.5), containing 1 mM EDTA, 7 M guanidine hydrochloride, and 20 mM 2-mercaptoethanol. The mixture was rotated at 4°C for 1.5 h, and then dialyzed 4 times against 20 mM Tris-HCl buffer (pH 7.5), containing 2 M NaCl and 2 mM 2-mercaptoethanol. The resulting histone octamer was purified by Superdex 200 gel-filtration column chromatography (GE healthcare). The H3.Y nucleosome was reconstituted with the histone octamer and the 146 base-pair or 193 base-pair DNA fragment by the salt dialysis method, as described previously (35). The H3.3 nucleosome was also prepared by the same method. The reconstituted nucleosomes were purified by non-denaturing 6% polyacrylamide gel electrophoresis, using a Prep Cell apparatus (Bio-Rad).

The heterotypic nucleosome containing H3.Y and H3.3 was prepared by the method described previously (29). Purified H2A, H2B, H3.Y, His_6-SUMO tagged H3.3, and H4 were mixed, and the histone octamers were prepared as described above. Three histone octamers, containing two H3.Y, one H3.Y and one His_6-SUMO tagged H3.3, or two His_6-SUMO tagged H3.3, were reconstituted. The nucleosomes were reconstituted with the mixture of histone octamers in the presence of the 146 base-pair or 193 base-pair DNA fragment, by the salt dialysis method. The three types of nucleosomes were then separated by non-denaturing 6% polyacrylamide gel electrophoresis, using a Prep Cell apparatus, and the heterotypic nucleosome was purified. After purification, the His_6-SUMO tag of H3.3 was cleaved by PreScission protease, and the resulting heterotypic H3.Y/H3.3 nucleosome was further purified using a Prep Cell apparatus.

For the thermal stability assay, the tetrasome containing H3.Y-H4 or H3.3-H4 was prepared by the salt-dialysis method, with the palindromic 146 base-pair satellite DNA fragment (2).

Crystallization and structure determination

The H3.Y nucleosome was concentrated to 2.5 mg/ml. The crystals of the H3.Y nucleosome were obtained by the hanging drop vapor diffusion method, by mixing equal volumes of the sample and the reservoir solution (100 mM sodium acetate (pH 4.6), 0.14 M $MnCl_2$, 12% 2-propanol, and 6% trimethylamine N-oxide dihydrate) at 20°C. Crystals were transferred into the cryoprotectant solution, containing 100 mM sodium acetate (pH 4.6), 0.14 M $MnCl_2$, 30% PEG400 and 2% trehalose at 4°C and were flash cooled in a stream of N_2 gas (100 K).

The data set was collected at the BL-17A beamline in the Photon Factory (KEK) and the BL41XU beamline in SPring-8. Data set indexing and scaling were performed with the HKL2000 program (36). The structure of the H3.Y nucleosome was solved by the molecular replacement method using the *Phaser* program (37), with the human nucleosome structure (PDB ID: 3AV2) as the guide. All refinements of the model were performed using the *PHENIX* program (38). The model was subjected to rigid body refinement in the initial refinement. After the rigid body refinement, iterative rounds of refinements, including the xyz coordinates, the real-space, the occupancies and the individual B-factors, were performed. Manual model building was performed using the *COOT* program (39). The final structure showed no outliers in the Ramachandran plot, as evaluated with the *MolProbity* program (Supplementary Table S1) (40). All structure figures were made using PyMOL (Schrödinger; http://www.pymol.org).

Micrococcal nuclease treatment assay

The nucleosomes containing either the 146 base-pair DNA (α-satellite derivative, 1.4 μg of DNA) or the 193 base-pair DNA containing the Widom601 sequence (1.4 μg of DNA) were incubated at 37°C for the indicated times, in the presence of 0.7 or 1.4 units of MNase (Takara), respectively, in 70 μl of reaction solution, containing 42 mM Tris-HCl (pH 8.0), 15 mM NaCl, 2.5 mM $CaCl_2$ and 1.8 mM

dithiothreitol. After the incubation, each aliquot (10 μl) was stopped by adding 15 μl of deproteinization solution (0.5 mg/ml proteinase K solution (Roche), containing 20 mM Tris-HCl (pH 8.0), 80 mM EDTA and 0.25% SDS). The reaction products were analyzed by non-denaturing 6% polyacrylamide gel electrophoresis in 0.2x TBE buffer (18 mM Tris base, 18 mM boric acid and 0.4 mM EDTA). The gel was stained with ethidium bromide. The band intensity of the undigested 146 base-pair DNA was quantitated with an LAS-4000 image analyzer (GE Healthcare), using MultiGauge ver. 3.2 (Fujifilm).

H1 binding assay and H1-nucleosome complex MNase treatment assay

The indicated amounts of H1 were mixed with the nucleosomes (0.1 μM), containing the 193 base-pair DNA in the presence of Nap1 (0.3 μM), in 10 μl of the reaction buffer, containing 35 mM Tris-HCl (pH 8.0), 70 mM NaCl, 0.01 mM PMSF, 0.05 mM EDTA, 5% glycerol, 1.2 mM dithiothreitol, 1.1 mM 2-mercaptoethanol and 5 μg/ml bovine serum albumin (BSA). The mixtures were incubated at 37°C for 30 min, to form the H1-nucleosome complex. The samples were then analyzed by non-denaturing 5% polyacrylamide gel electrophoresis in 1x TBE buffer (90 mM Tris base, 90 mM boric acid and 2 mM EDTA). The gel was stained with ethidium bromide. The band intensities of the H1-nucleosome complexes and nucleosomes were quantitated with a LAS-4000 image analyzer (GE healthcare) using MultiGauge ver. 3.2 (Fujifilm) and the H1-nucleosome complex formation rate was calculated.

For the MNase treatment assay with the H1-nucleosome complex, the sample (30 μl) containing H1.2 was incubated with MNase (1.05 units) at 37°C for the indicated times, in the presence of $CaCl_2$ (2.5 mM). The reaction was conducted in a 45 μl reaction mixture. After the incubation, each aliquot (10 μl) was stopped by adding 10 μl of deproteinization solution (0.5 mg/ml proteinase K solution (Roche), containing 20 mM Tris-HCl (pH 8.0), 80 mM EDTA and 0.25% SDS). The DNAs were extracted by phenol/chloroform/isoamyl alcohol, followed by ethanol precipitation, and were analyzed by non-denaturing 6% polyacrylamide gel electrophoresis in 0.2x TBE buffer (18 mM Tris base, 18 mM boric acid and 0.4 mM EDTA). The gel was stained with ethidium bromide.

Hydroxyl radical footprinting

The 193 base-pair 601 DNA was dephosphorylated by alkaline phosphatase (Takara), and cleaved by HinfI (Takara). The resulting 164 base-pair DNA fragment was purified by TSK gel DEAE-5PW (TOSOH) anion exchange column chromatography. The purified 164 base-pair DNA fragment was ligated with a 5′-Cy5 labeled 29 base-pair double stranded oligonucleotide, to generate the 5′-Cy5 labeled 193 base-pair DNA fragment (193 bp Cy5 DNA). Nucleosomes were then reconstituted with the 193 bp Cy5 DNA by the salt dialysis method. The reconstituted nucleosomes were purified by non-denaturing 6% polyacrylamide gel electrophoresis, using a Prep Cell apparatus. Hydroxyl radical footprinting experiments were performed by the method described previously, with modifications (41,42). H1.2 (0.9 μM) and the nucleosome (0.5 μM) were mixed in the presence of Nap1 (1.5 μM) in the reaction mixture (60 μl), and the H1-nucleosome complexes were prepared by the Nap1-mediated method. The samples were exchanged into quencher-free buffer (5 mM Tris-HCl (pH 7.5), 5 mM NaCl and 0.25 mM EDTA) by filtration, using an Amicon Ultra 30 kDa filter (Millipore). For the hydroxyl radical reaction, the H1-nucleosome complex (1.5 μg of DNA) in 50 μl was placed at the bottom of a 1.5 ml tube. Aliquots of 4 mM $FeAmSO_4$/8 mM EDTA (2.5 μl), 0.1 M sodium ascorbate (2.5 μl) and 0.6% v/v (2.5 μl) hydrogen peroxide were placed on the wall of the tube. The reaction was initiated by mixing these reagents by centrifugation, and after 2 min at room temperature, the reactions were terminated by adding 5 μl of 100 mM thiourea and 10 μl of 3 M sodium acetate (pH 5.2). The DNAs were extracted by phenol/chloroform/isoamyl alcohol, precipitated with ethanol/glycogen and fractionated on an 8% polyacrylamide urea denaturing gel. The end labeled Cy5 fluorescence signal was detected through a glass plate on a Typhoon 9410 imager (GE Healthcare).

Thermal stability assay

The nucleosomes (0.45 μg of DNA) or the tetrasomes (0.45 μg of DNA) containing the 146 base-pair DNA were subjected to the thermal stability assay (43). The thermal stability assay was conducted in 20 μl of 20 mM Tris-HCl (pH 7.5) buffer, containing 5x SYPRO Orange, 1 mM dithiothreitol and 100 mM NaCl. The StepOnePlus™ Real-Time PCR unit (Applied Biosystems) was used to detect the fluorescence signals with a temperature gradient from 26 to 95°C, in steps of 1°C/min. Normalization of the fluorescence intensity was performed as follows: $F(T)_{normalized} = [F(T) - F(26)] / [F(95) - F(26)]$. F(T) indicates the fluorescence intensity at a particular temperature.

Preparation of the H3.3 and H3.Y nucleosome arrays

The 12 tandem repeats of the 208 base-pair Widom601 DNA were purified by the method described previously (44). The fragment containing 12 repeats of the 601 sequence was isolated by EcoRV digestion, and was purified by polyethylene glycol precipitation. The nucleosome arrays were reconstituted using the prepared histone octamers with the 12 repeat 601 DNA, by the salt dialysis method. The reconstituted nucleosome arrays were further purified by 0.7% agarose-2% acrylamide composite gel electrophoresis, using a Prepcell apparatus. The nucleosome occupancy on the 601 DNA sequences was evaluated by digestion with the restriction enzyme ScaI, which cleaves the linker DNA regions of the nucleosome array. Briefly, purified nucleosome array samples (100 ng of DNA) were digested by ScaI (Takara) in a 10 μl reaction solution (10 mM Tris-HCl (pH 7.5), 50 mM NaCl, 0.5 mM $MgCl_2$ and 0.1 mg/ml BSA) at 22°C for 12 h, and the resulting mononucleosomes were analyzed by electrophoresis on a non-denaturing 5% polyacylamide gel in 1x TBE buffer (90 mM Tris base, 90 mM boric acid and 2 mM EDTA), with ethidium bromide staining. The gel image was acquired with an LAS-4000 image analyzer (GE Healthcare).

Analytical ultracentrifugation sedimentation velocity assay

The nucleosome arrays (OD_{260} = 0.6–0.8) were dialyzed against a solution containing 10 mM Tris-HCl (pH 7.5), in the presence or absence of 1 mM $MgCl_2$. The sedimentation velocity analysis was performed with a Beckman Coulter ProteomeLab XL-I, using an 8-hole An-50Ti rotor. Before the sedimentation analysis, the samples were incubated for 2 h at 20°C. The sedimentation velocity assay was performed at 22 000 rpm, and scans at 260 nm were collected. The data were analyzed by the enhanced van Holde–Weischet method (45), using *UltraScan*II 9.9, revision 1927 (Demeler, http:/www.ultrascan.uthscsa.edu). The sedimentation coefficient $S_{20,w}$ was calculated with a partial specific volume of 0.65 ml/g. The buffer density and viscosity were adjusted to the buffer solution.

Fluorescence recovery after photobleaching (FRAP)

The DNA fragments encoding H3.Y and H3.3 were ligated into the pEGFP-C3 vector (Clontech). To establish stable cell lines expressing H3.Y or H3.3 as the N-terminal GFP-fusion proteins, HeLa cells were transfected with the EGFP vector containing H3.Y or H3.3, using Lipofectamine 2000 (Life Technologies), and were selected with 1 mg/ml G418 (Nacalai Tesque). To measure the expression-level range of GFP-H3.3 and GFP-H3.Y, the fluorescent intensities of about 1000 HeLa cells were obtained using a fluorescence microscope (Ti-E; Nikon), and were analyzed using the NIS software (Nikon). For the FRAP analysis, cells were grown on a glass-bottom dish (Mat-tek) in Dulbecco's modified Eagle's medium (DMEM), supplemented with 10% fetal calf serum, 50 μg/ml streptomycin and 10 Units/ml penicillin. The FRAP analysis was performed in the presence of 100 μg/ml cycloheximide, to prevent new protein synthesis, using an FV-1000 confocal microscope (Olympus), as described previously (46). An 800 x 800 pixels-image of a confocal field, containing ∼10 nuclei, was collected with a 60x UPlanSApo NA = 1.35 lens (scan speed 2 μs/pixel, zoom 2, 0.2% transmission of 488-nm Ar laser, LP505 emission filter, pinhole 800 μm and Kalman filtration for four scans). One-half of each nucleus was then photobleached using 90% transmission of the 488-nm laser (two iterations), and images were collected using the original settings at 5 min intervals for 100 min. The collected images were exported as TIFF files, and the fluorescence intensities of the bleached and unbleached areas were measured using Image J 1.46r (Rasband, http://rsb.info.nih.gov/ij/). After background subtraction, the intensity of the bleached area relative to that of the unbleached area was calculated.

Analysis of the GFP-H3.Y incorporation into chromatin

HeLa cells, in which GFP-H3.Y or GFP-H3.3 was exogenously expressed, were washed with ice-cold RSB (10 mM HEPES-NaOH (pH 7.4), 1.5 mM $MgCl_2$ and 15 mM NaCl). The cells were collected and resuspended in 4 ml of ice-cold RSB, containing 1% Triton X-100 and 1x protease inhibitor (cOmplete, EDTA-free, Roche). The cells were disrupted by homogenization with a Dounce homogenizer (tight pestle; 10 times). Nuclei were collected by centrifugation (956 x*g*; 5 min; 4°C), washed twice with 1 ml of buffer A (15 mM HEPES-NaOH (pH 7.4), 15 mM NaCl, 60 mM KCl, 0.34 M sucrose, 0.15 mM spermidine, 0.5 mM spermine, 1 mM dithiothreitol and 1x protease inhibitor), and resuspended in buffer A (10x volume of pellet; ∼5 x 10^7 nuclei/ml). $CaCl_2$ (final 1 mM, 1.3 ml) was added to 1.3 ml of the nuclear suspension, and then micrococcal nuclease (6.3 μl, New England Biolabs; 2 x 10^6 Gel units/ml; stock in 10 mM Tris-HCl (pH 7.5), 50 mM NaCl, 1 mM EDTA, 50% glycerol) was added (9600 Gel units/ml). The sample was incubated at 30°C for 1 h (mixing by inversion every 15 min). After adding 26 ml of 0.5 M EDTA (pH 8.0) and centrifuging the solution (10 621 x*g*; 10 min; 4°C), the pellet was suspended in 450 μl of 10 mM EDTA (pH 8.0). Subsequently, 5 M NaCl (50 μl) was added to the sample, which was centrifuged (20 000 x*g*; 10 min; 4°C). The supernatant was then collected as the chromatin fraction.

For immunoprecipitation, Dynabeads Protein G (50 μl, Life Technologies) was previously washed three times with 1 ml of buffer B (20 mM Tris-HCl (pH 8.0), 500 mM NaCl, 5 mM EDTA, and 0.2% Tween 20), and was mixed with buffer B (100 μl) and anti-GFP pAb (2 μl, MBL) at 25°C for 3 h. After washing the beads with 1 ml of buffer B, 440 μl of the chromatin fraction was added, and the mixture was incubated overnight at 4°C with rotation. The beads were then washed 3 times with 1 ml of buffer B, and the proteins were eluted by adding 50 μl of 2x SDS buffer (100 mM Tris-HCl (pH 6.8), 4% SDS, 20% glycerol, 0.2% bromophenol blue and 100 mM dithiothreitol). Afterward, the sample was incubated at 60°C for 1 h. For DNA analysis, DNA was purified using a QIAquick PCR Purification Kit (Qiagen), and was analyzed by electrophoresis on a 2% agarose gel in 1x TAE buffer (40 mM Tris-acetate and 1 mM EDTA), with GelRed(Biotium) staining. For protein analysis, the samples were separated by 15% SDS-PAGE in 1x SDS buffer (25 mM Tris-HCl (pH8.3), 184 mM glycine and 0.1% SDS), and the proteins were detected by CBB staining and Western blotting with a peroxidase-conjugated anti-GFP mAb (1:1000; Nacalai Tesque; 05178-34). The gel image was acquired with an LAS-3000 image analyzer (GE Healthcare).

ChIP-seq and mRNA-seq

The mRNA-seq library was prepared using a TruSeq RNA-Seq sample preparation kit (Illumina K.K.; USA), and the samples were sequenced on an Illumina HiSeq1500 system. The gene expression levels (FPKM; Fragments per kilobase of exon per million mapped sequence reads) were estimated using the Tophat (version 2.0.8) and Cufflinks (version 2.0.1) programs with the default parameters (47). The eleven expression level groups, named *Zero*, q0-10th, q10-20th … and q90-100th, were defined according to the FPKMs of the genes. The members of the *Zero* group have exactly FPKM = 0, and the others were divided into 10 groups with the deciles of all FPKMs; i.e. the genes were sorted by the FPKMs and assigned into 10 equal groups.

The ChIP-seq library was prepared as described previously (48). The samples were sequenced on an Illumina HiSeq1500 system. The sequenced reads were mapped onto the human genome (hg19) with the Bowtie program (version 2.2.2), using the default parameters, and the unique-hit reads were utilized for further analysis (see Supple-

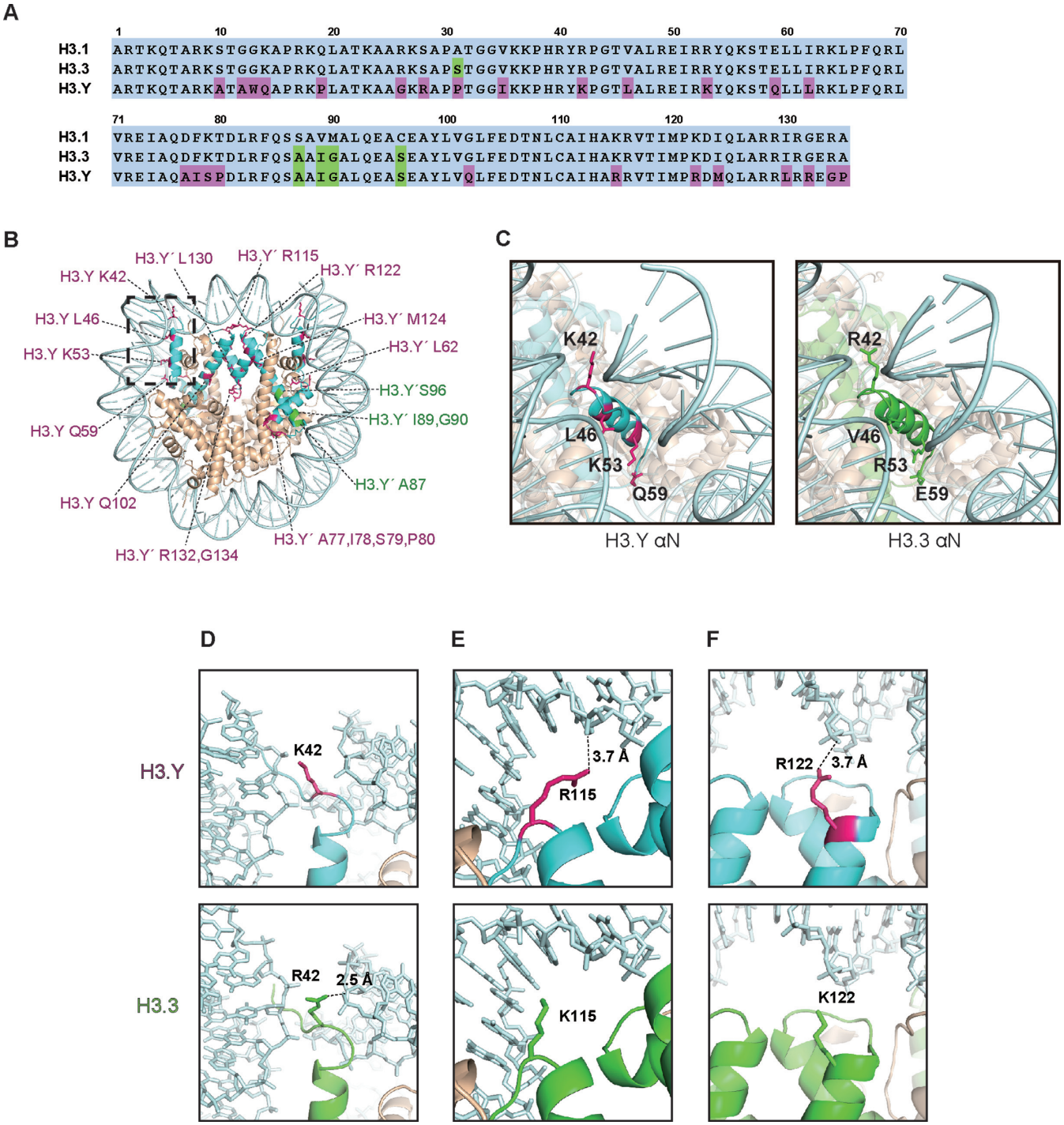

Figure 1. Structure of the human H3.Y nucleosome. (**A**) Amino acid sequence alignment of the human H3.1, H3.3 and H3.Y proteins. The H3.Y-specific residues are colored purple, and the residues conserved between H3.3 and H3.Y are colored green. (**B**) Crystal structure of the human H3.Y nucleosome. The H3.Y molecules are colored light blue. The H3.Y-specific residues are represented by purple letters, and the residues conserved between H3.3 and H3.Y are represented by green letters. (**C**) Close-up views of the αN regions of the H3.Y and H3.3 nucleosomes. The H3.Y αN region encircled by the dotted square in panel B is enlarged and presented with a modified angle (left panel). The H3.Y-specific residues corresponding to K42, L46, K53 and Q59, which are located in the αN region, are colored purple. The H3.3 (green) αN region is also presented with the same angle as in the left panel (right panel) (PDB ID: 3AV2). (**D, E** and **F**) Close-up views of the H3.Y-specific (D) Lys42, (E) Arg115 and (F) Arg122 residues (left panels), corresponding to the H3.3 Arg42, Lys115 and Lys122 residues (middle panels). The right panels show the merged views of these residues of the H3.Y and H3.3 nucleosomes.

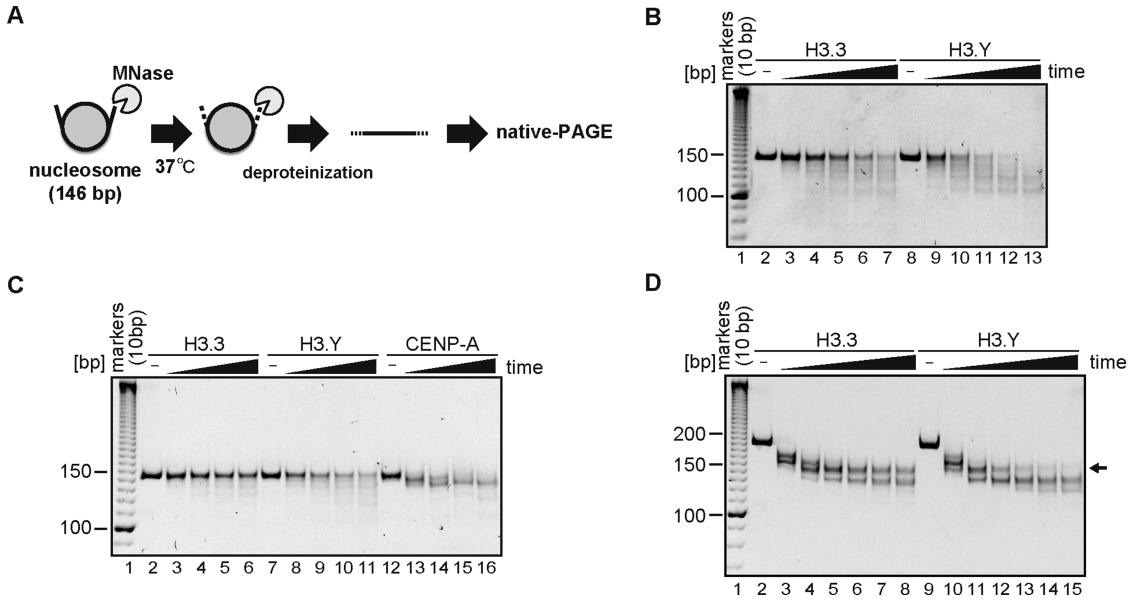

Figure 2. DNA end flexibility of the H3.Y nucleosome. (**A**) Schematic representation of the MNase treatment assay. The flexible DNA ends of the nucleosome are preferentially digested by MNase. After deproteinization, the remaining DNA fragments were analyzed by non-denaturing PAGE with ethidium bromide staining. (**B**) MNase treatment assay. The H3.3 (lanes 2–7) or H3.Y (lanes 8–13) nucleosomes containing a 146 base-pair DNA (α-satellite derivative) were treated with MNase for 0, 3, 6, 9, 12 and 15 min at 37°C. After the incubation, the reactions were stopped by adding proteinase K solution, containing SDS and EDTA. The reaction products were analyzed by non-denaturing 6% PAGE with ethidium bromide staining. The gel image shown is a representative of four independent experiments with similar results. Other experiments are shown in Supplementary Figure S2B, C and Figure 8A. (**C**) The H3.3 (lanes 2–6), H3.Y (lanes 7–11) and CENP-A (lanes 12–16) nucleosomes containing a 146 base-pair DNA were treated with MNase for 0, 90, 180, 270 and 360 s at 37°C. After the incubation, the reactions were stopped by adding a proteinase K solution, containing SDS and EDTA. The reaction products were analyzed by non-denaturing 6% PAGE with ethidium bromide staining. The gel image shown is a representative of three independent experiments with similar results. (**D**) The H3.3 (lanes 2–8) or H3.Y (lanes 9–15) nucleosomes containing the Widom601 193 base-pair DNA were treated with MNase for 0, 3, 6, 9,12, 15 and 18 min at 37°C. After the incubation, the reactions were stopped by adding the proteinase K solution, containing SDS and EDTA. The reaction products were analyzed by non-denaturing 6% PAGE with ethidium bromide staining. The arrow indicates the bands (about 150 base-pairs) corresponding to the nucleosome core particle. The gel image shown is a representative of three independent experiments with similar results.

mentary Table S2 for read number statistics). The normalized ChIP-Seq signal intensities were calculated, as follows. To calculate the signal intensity of the ChIP-seq data, we first counted the mapped reads on a 1000 base-pair stretch with 10% overlapping windows (bins) throughout the human genome, and then the counts were normalized as Reads Per Kilobases Per Million reads (RPKMs) (49). The input-normalized ChIP-Seq signal intensities were calculated as the RPKM differences between the ChIP and input DNA-control data (ChIP–input) on each bin. The ChIP-seq peaks of GFP-H3.Y were identified using MACS (version 2.0.10) (50) with the following parameters: callpeak–gsize hs–nomodel–broad–extsize 144–to-large–*P* value 1e-3.

RESULTS

Human histone H3.Y forms nucleosomes with flexible DNA ends

H3.Y is a distant histone H3 variant, in which 26 and 30 amino acid residues differ from H3.3 and H3.1, respectively (Figure 1A). To study the nucleosome containing H3.Y, we purified the human histones, H2A, H2B, H4 and H3.Y (Supplementary Figure S1A). The H3.Y nucleosome was efficiently reconstituted by the salt dialysis method (Supplementary Figure S1B and S1C). We then determined the crystal structure of the H3.Y nucleosome at 2.8 Å resolution (Figure 1B). Interestingly, we found that four H3.Y-specific amino acid residues, Lys42, Leu46, Lys53 and Gln59, are located near the DNA ends of the nucleosome (Figure 1C). Among these, the H3.Y Lys42 residue, which corresponds to the H3.3 Arg42 residue, may affect the DNA binding, because the H3.3 Arg42 side chain, but not the H3.Y Lys42 side chain, directly binds to the DNA in the H3.3 nucleosome (Figure 1D). In H3.Y, the Arg115 and Arg122 side chains, which correspond to the H3.3 Lys115 and Lys122 side chains, may directly interact with the DNA (Figure 1E and F). The H3.3 Lys115 and Lys122 side chains reportedly form water-mediated hydrogen bonds with the DNA backbone around the nucleosomal dyad (51). These results suggested that, in the H3.Y nucleosome, the histone-DNA contacts may differ from those in the H3.3 nucleosome.

To test the DNA end flexibility of the H3.Y nucleosome, we performed a micrococcal nuclease (MNase) treatment assay (Figure 2A). In this assay, the DNA regions that are flexibly detached from the histone surface are digested by MNase. Interestingly, the 146 base-pair DNA (α-satellite derivative) in the H3.Y nucleosome was more susceptible to MNase digestion than that in the H3.3 nucleosome (Figure 2B), indicating that the DNA ends of the H3.Y nucleosome are more flexible than those of the H3.3 nucleosome. In a comparison with the CENP-A nucleosome, which is known to have flexible DNA ends (52–55), we found that the DNA ends of the H3.Y nucleosome were less susceptible to MNase digestion than those of the CENP-A nu-

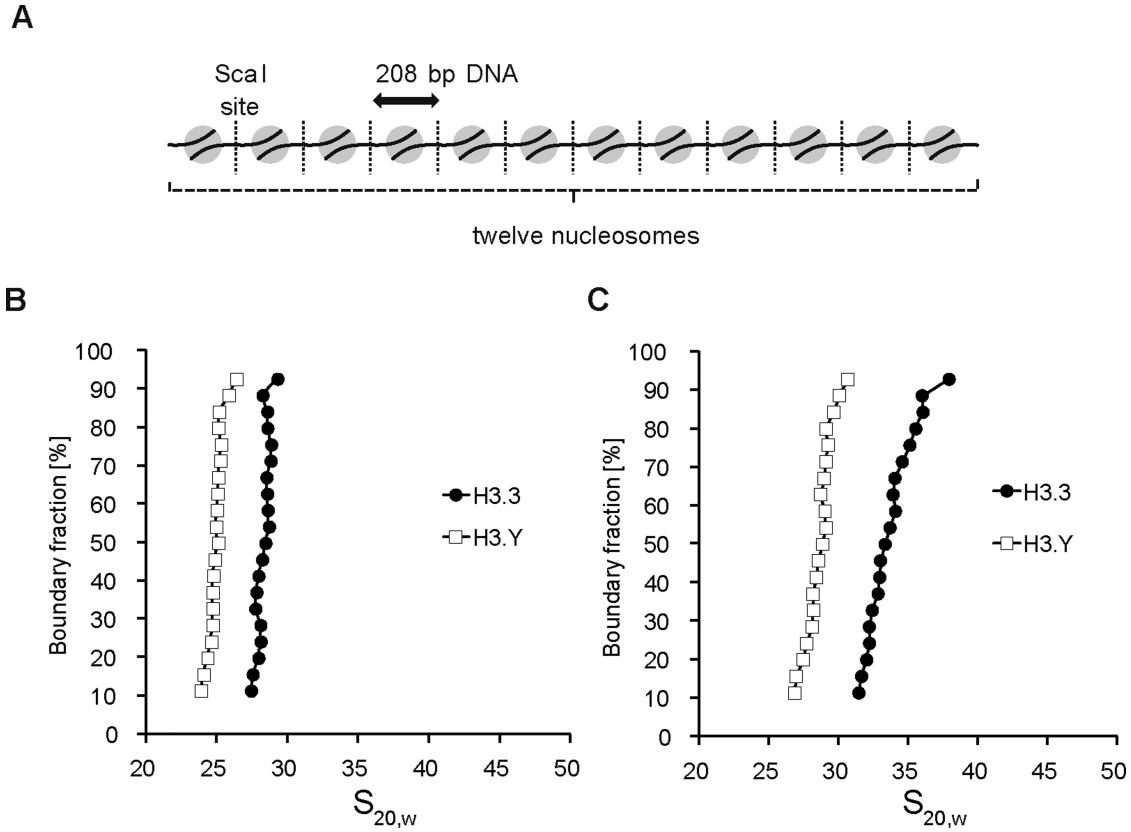

Figure 3. H3.Y forms chromatin with the relaxed configuration. (**A**) Schematic representation of the nucleosome array reconstituted with 12 repeats of a 208 base-pair Widom601 DNA. (**B** and **C**) Analytical ultracentrifugation sedimentation velocity analyses of the H3.Y and H3.3 nucleosome arrays in the (B) absence or (C) presence of 1 mM $MgCl_2$. The distribution of the sedimentation coefficients was determined by the enhanced van Holde–Weischet method. Three independent experiments were performed, and the consistency of the results was confirmed.

cleosome (Figure 2C). Therefore, the DNA end flexibility of the H3.Y nucleosome is not significant, as compared to that of the CENP-A nucleosome. These differences in the DNA end flexibility resulted in the migration difference on an 8% polyacrylamide gel (run at 150 V for 4 h, Supplementary Figure S2A), although the difference was not easily detectable on a 6% polyacrylamide gel (run at 150 V for 1 h, Supplementary Figure S1B). In addition, we repeated the MNase assay with a 193 base-pair DNAs containing the Widom601 sequence, and confirmed that the results are perfectly consistent with those obtained with the 146 base-pair α-satellite DNA data (Figure 2D). This result indicates that the flexible DNA character of the H3.Y nucleosome is not due to the specific DNA sequence and length, but is a consequence of the intrinsic properties of H3.Y.

The H3.Y nucleosome forms a relaxed chromatin configuration

The DNA end flexibility of the H3.Y nucleosome may affect the higher order chromatin configuration. To test this possibility, we reconstituted nucleosome arrays with H3.Y or H3.3, consisting of 12 nucleosomes assembled on tandem repeats of the Widom601 DNA sequence (208 base pairs) (Figure 3A and Supplementary Figure S3A). The H3.Y and H3.3 nucleosome arrays were both efficiently reconstituted, as shown by the restriction enzyme (ScaI) digestion analysis; only trace amounts of the nucleosome-free 601 DNA segments were detected (Supplementary Figure S3B).

We then performed a sedimentation assay by analytical ultracentrifugation (44). Consistent with the previous data (56,57), the H3.3 nucleosome array exhibited sedimentation values of 27S-30S in the absence of Mg^{2+} ion (Figure 3B). Interestingly, we found that the H3.Y nucleosome array sedimented more slowly (24S-26S) (Figure 3B). This indicated that the H3.Y nucleosome actually contained the flexible DNA ends, and adopted a more relaxed configuration than the H3.3 nucleosome in the nucleosome array. As the nucleosome array becomes compacted in the presence of Mg^{2+} ion (58,59), we repeated the sedimentation assay in the presence of a physiological concentration (1 mM) of $MgCl_2$. As shown in Figure 3C, the S values of the H3.3 and H3.Y nucleosome arrays both substantially increased, probably due to their higher compaction. Importantly, the H3.Y nucleosome array still exhibited lower sedimentation values than the H3.3 nucleosome array, in the presence of 1 mM $MgCl_2$ (Figure 3C). Therefore, we concluded that the flexible DNA ends of the H3.Y nucleosome render a more relaxed chromatin configuration.

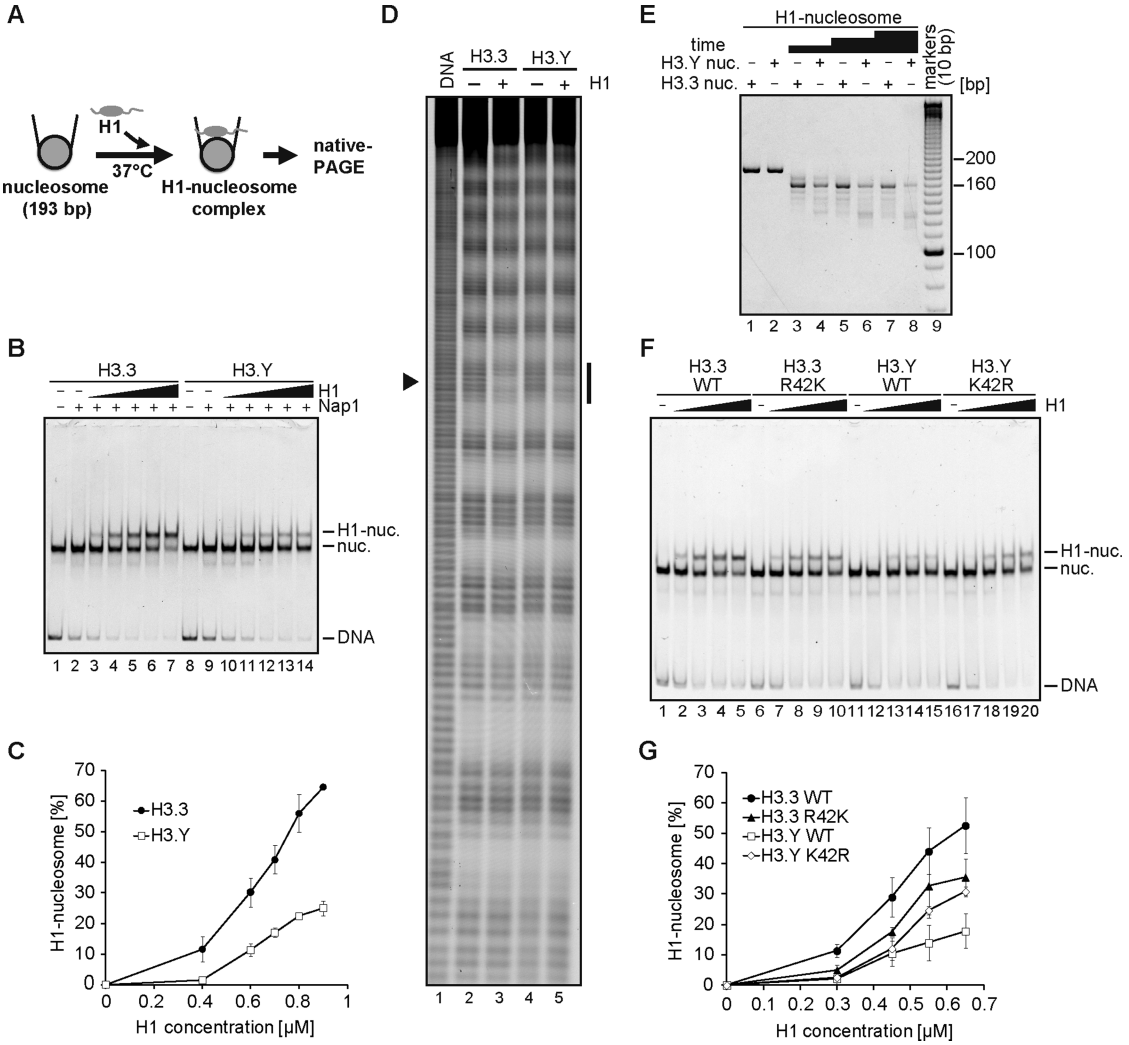

Figure 4. Linker histone H1 binding to the H3.Y nucleosome. (**A**) Schematic representation of the H1 binding assay. (**B**) Representative gel image of the H1 binding assay. Increasing amounts of H1 (0 μM: lanes 1, 2, 8 and 9; 0.4 μM: lanes 3 and 10; 0.6 μM: lanes 4 and 11; 0.7 μM: lanes 5 and 12; 0.8 μM: lanes 6 and 13; 0.9 μM: lanes 7 and 14) were mixed with H3.3 (lanes 1–7) or H3.Y (lanes 8–14) nucleosomes (0.1 μM) in presence of Nap1 (0.3 μM). After an incubation at 37°C, the complexes were detected by non-denaturing 5% PAGE with ethidium bromide staining. (**C**) Graphical representation of the H1 binding assay. The band intensities corresponding to the H1-nucleosome complex and nucleosomes were quantitated, and the rate of H1-nucleosome complex formation was plotted against the H1 concentration. The error bars indicate standard deviations (n = 3). (**D**) Hydroxyl radical footprinting of the H1-nucleosome complexes. The H3.Y and H3.3 nucleosomes were reconstituted with the 5′-Cy5 labeled 193 base-pair 601 DNA, and were purified by non-denaturing 6% polyacrylamide gel electrophoresis. Lane 1 indicates a control experiment with naked DNA. The H3.3 (lanes 2–3) or H3.Y (lanes 4–5) nucleosomes were subjected to hydroxyl radical attack in the presence (lanes 3 and 5) or absence (lanes 2 and 4) of histone H1.2. The DNA samples were then resolved on an 8% denaturing polyacrylamide gel. The arrowhead (left) and the black bar (right) indicate the nucleosomal dyad and the footprint of H1.2, respectively. (**E**) MNase treatment assay of the H1-nucleosome complex. The H1-nucleosome complex containing the H3.3 (the complex formation rate: 77%, lanes 1, 3, 5 and 7) or H3.Y nucleosome (the complex formation rate: 49%, lanes 2, 4, 6 and 8) was treated with MNase for 0, 3, 6 and 9 min for 37°C. After the incubation, the reactions were stopped by adding the proteinase K solution, containing SDS and EDTA. The DNAs were extracted, and were analyzed by non-denaturing 6% PAGE with ethidium bromide staining. (**F**) Representative gel image of the H1 binding assay with the H3.3 R42K and H3.Y K42R nucleosomes. Increasing amounts of H1 (0 μM: lanes 1, 6, 11 and 16; 0.3 μM: lanes 2, 7, 12 and 17; 0.45 μM: lanes 3, 8, 13 and 18; 0.55 μM: lanes 4, 9, 14 and 19; 0.65 μM: lanes 5, 10, 15 and 20) were mixed with H3.3 (lanes 1–4), H3.3 R42K (lanes 5–10), H3.Y (lane 11–15) or H3.Y K42R (lanes 16–20) nucleosomes (0.1 μM), in the presence of Nap1 (0.3 μM). After the incubation at 37°C, the complexes were detected by non-denaturing 5% PAGE with ethidium bromide staining. (**G**) Graphical representation of the H1 binding assay of the amino acid 42 mutants. The error bars indicate standard deviations (n = 3).

Linker histone H1 binds less efficiently to the H3.Y nucleosome

The linker histone H1 preferentially binds to nucleosomal DNA, and compacts chromatin into a higher-ordered structure. We tested the binding of histone H1 to the H3.3 and H3.Y nucleosomes containing a 193 base-pair DNA fragment, using a gel mobility shift assay (Figure 4A). In this assay, we conducted the H1-nucleosome binding in the presence of a histone chaperone, Nap1, which properly loads the linker histone on the nucleosome (31,41,60,61). The reactions were conducted under the standard conditions (35 mM Tris-HCl, 70 mM NaCl, 0.01 mM PMSF, 0.05 mM EDTA, 5% glycerol, 1.2 mM dithiothreitol, 1.1 mM

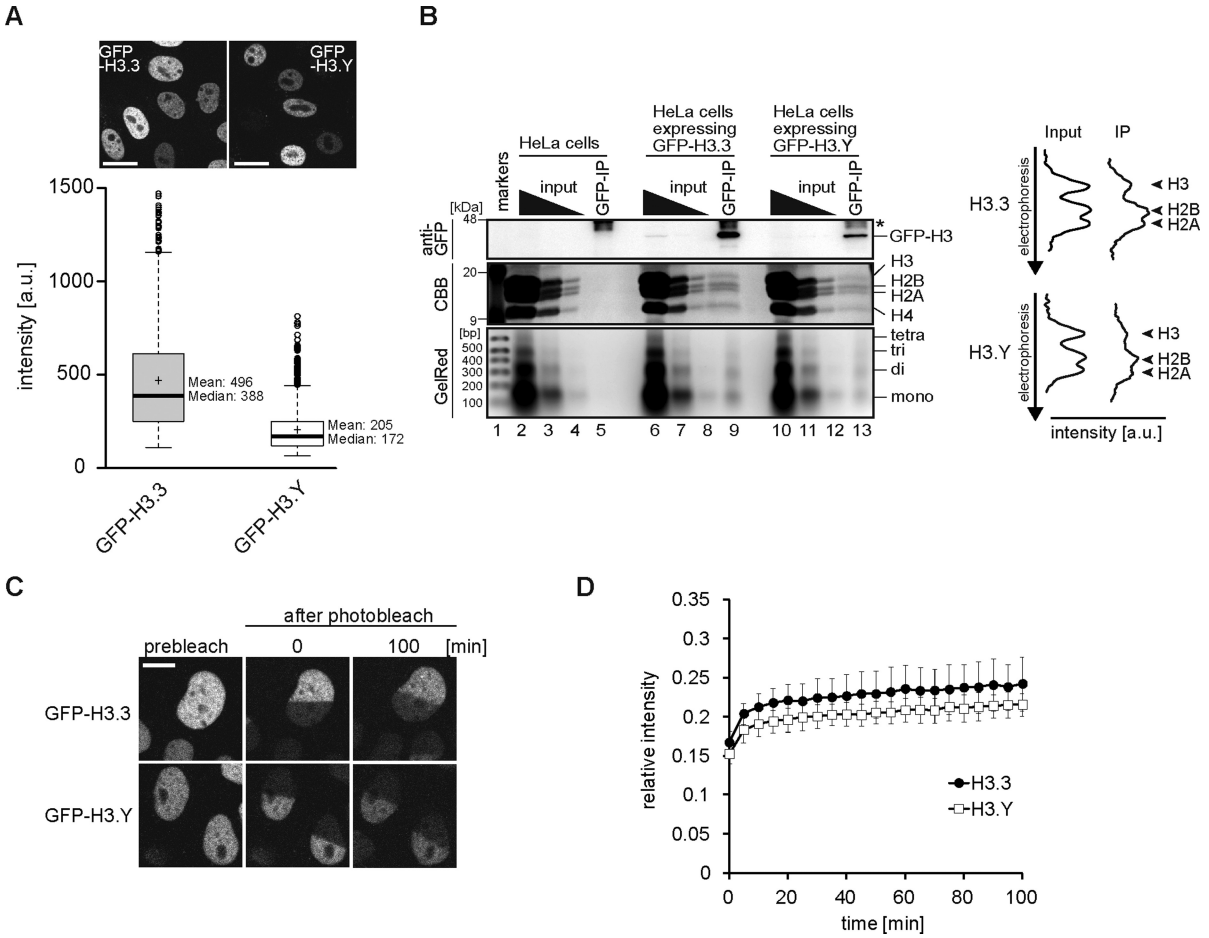

Figure 5. Stability of the H3.Y nucleosome *in vivo*. (**A**) Boxplots representing the distribution of fluorescent intensities in HeLa cells stably expressing GFP-H3.3 (n = 800) and GFP-H3.Y (n = 800). The outlier is indicated as a white circle. The upper panels show representative images of HeLa cells expressing GFP-H3.3 (left) and GFP-H3.Y (right), respectively. The scale bar indicates 20 μm. (**B**) Native chromatin immunoprecipitation experiment. Nucleosome fractions from HeLa cells without and with GFP-H3.3 or GFP-H3.Y expression were immunoprecipitated using an anti-GFP antibody. The input (1/1, 1/10 and 1/100 dilutions) and immunoprecipitated samples from HeLa cells (lanes 2–5), and HeLa cells expressing GFP-H3.3 (lanes 6–9), or GFP-H3.Y (lanes 10–13), were separated by 15% SDS-PAGE, and were either blotted onto a membrane before detection using an anti-GFP antibody (top) or stained by Coomassie Brilliant Blue (middle). The indicated DNA fragments of the input (1/1, 1/10, 1/100 dilutions) and the immunoprecipitated samples were analyzed by 2% agarose gel electrophoresis with GelRed staining (bottom). The line intensity profiles of histones stained by Coomassie Brilliant Blue are shown. (**C**) Fluorescence recovery after photobleaching (FRAP) analysis in HeLa cells. The mobility of GFP-fused H3.3 or H3.Y was analyzed by bleaching one-half of a nucleus in the presence of 100 μg/ml cycloheximide. Representative images for GFP-H3.3 and GFP-H3.Y are presented in the upper and lower panels, respectively. The bar indicates 10 μm. (**D**) Graphical representation of the FRAP experiments shown in panel A. The average relative fluorescence intensities of GFP-H3.3 (n = 10) and GFP-H3.Y (n = 10) are shown, with the standard deviations.

2-mercaptoethanol and 5 μg/ml BSA). As expected, H1 efficiently bound to the H3.3 nucleosome (Figure 4B, lanes 1–7 and C). When the H3.Y nucleosome was mixed with H1, smaller amounts of the H1-nucleosome complexes (chromatosomes) were observed, as compared to the H3.3 nucleosome, under the standard conditions (Figure 4B, lanes 10–14 versus lanes 3–7). For example, in the presence of 0.9 μM H1, 65% of the H3.3 nucleosome formed the complexes with H1, but only 25% of the H3.Y nucleosome did so (Figure 4C). These results suggest that H1 binds less efficiently to the H3.Y nucleosome. We found that, under the low salt conditions (5 mM Tris-HCl, 5 mM NaCl and 0.25 mM EDTA), the H1 binding to the H3.Y nucleosome was enhanced, and the difference in the H1 binding between the H3.Y and H3.3 nucleosomes became smaller (Supplementary Figure S4). To ensure that H1 properly binds to the H3.Y nucleosome, we then performed hydroxyl radical footprinting experiments under the low salt conditions. We found that, in the H3.Y nucleosome, DNA protection around the dyad axis was observed in the presence of H1, as well as in the H3.3 nucleosome (Figure 4D). Consistently, the MNase treatment assay revealed that the bands corresponding to the chromatosomes were clearly observed in both the H3.Y and H3.3 nucleosomes (Figure 4E). These results confirmed that the linker histone H1 properly binds to the H3.Y nucleosome, although the H1 binding to the H3.Y nucleosome is less efficient than that to the H3.3 nucleosome (Figure 4B and C).

We next tested whether the H3.Y-specific amino acid residue is actually involved in the reduced H1 binding to the H3.Y nucleosome under the standard conditions. To do so, we focused on the H3.3 Arg42 residue, which is located

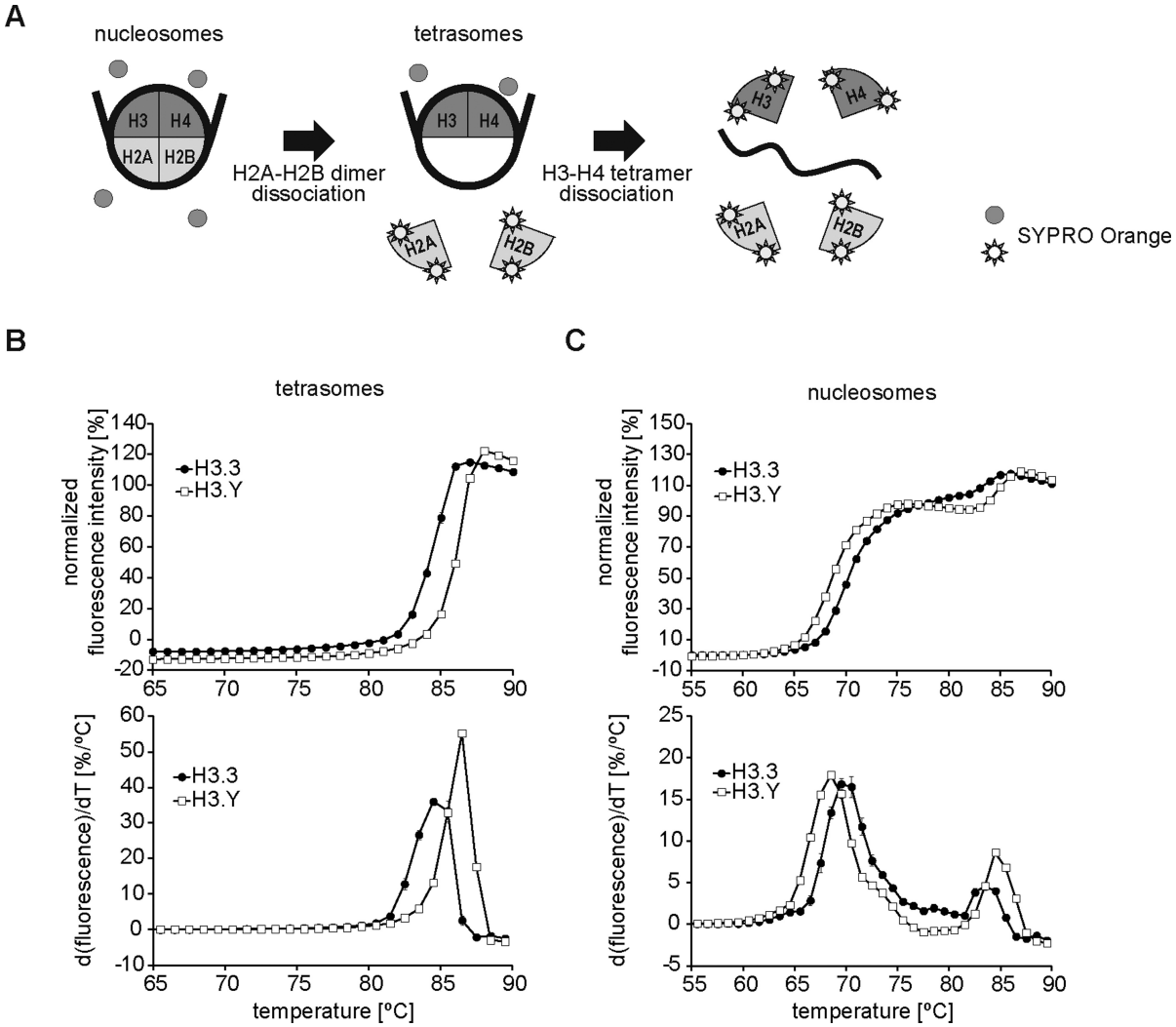

Figure 6. Thermal dissociation of the H2A–H2B dimer and the H3.Y–H4 tetramer from DNA. (**A**) Schematic representation of the thermal stability assay. In this assay, histones thermally dissociated from the nucleosomes or the tetrasomes were measured by detecting the fluorescence of SYPRO Orange fluorescent dye, which hydrophobically binds to the denatured histones. (**B**) Normalized fluorescence intensity curves of the thermal dissociation of the H3–H4 tetramers containing H3.3 or H3.Y (upper panel), with plots of the derivatives of the curves (lower panel). The error bars indicate standard deviations (n = 3). (**C**) Normalized fluorescence intensity curves of thermal disruption of the nucleosomes containing H3.3 or H3.Y (upper panel), with plots of the derivatives of the curves (lower panel). The first and second peaks correspond to the dissociations of the H2A–H2B dimer and the H3–H4 tetramer from the nucleosome, respectively. The error bars indicate standard deviations (n = 3).

near the entry/exit sites of the nucleosome (Figure 1D). This residue is substituted by Lys42 in H3.Y (Figure 1A). We then purified the H3.3 R42K and H3.Y K42R mutants, in which the corresponding residues are replaced with each other. As compared to the wild-type H3.3 nucleosome, H1 bound less efficiently to the H3.3 R42K nucleosome (Figure 4F and G). As expected, the H1 binding to the H3.Y K42R nucleosome is enhanced, as compared to the wild-type H3.Y nucleosome (Figure 4F and G). These results consistently indicate that the H3.Y-specific Lys42 residue actually functions to reduce the H1-nucleosome binding. It should be noted that the effects of the H3.3 R42K and H3.Y K42R mutations in the H1-nucleosome binding are partial, suggesting that other residues also contribute to the characteristics of the H3.Y nucleosome.

H3.Y is stably incorporated into chromatin *in vivo*, and forms stable nucleosomes *in vitro*

As described above, the H3.Y nucleosome contains flexible DNA segments at the ends. We studied the H3.Y nucleosome stability *in vivo,* by monitoring the H3.Y mobility in living cells. HeLa cell lines that stably expressed the green fluorescent protein (GFP)-fused H3.Y (GFP-H3.Y) and H3.3 (GFP-H3.3, as a control) were established. The expression level of GFP-H3.Y was about one-half of that of GFP-H3.3 (Figure 5A). To determine whether GFP-H3.Y was incorporated into chromatin, nucleosome fractions were prepared from these HeLa cells, and immunoprecipitated using an anti-GFP antibody. Both GFP-H3.Y and GFP-H3.3 were recovered in the immunoprecipitated nucleosomes, in which the stoichiometry of the endogenous H3 was reduced, as compared to the input (Figure 5B). This re-

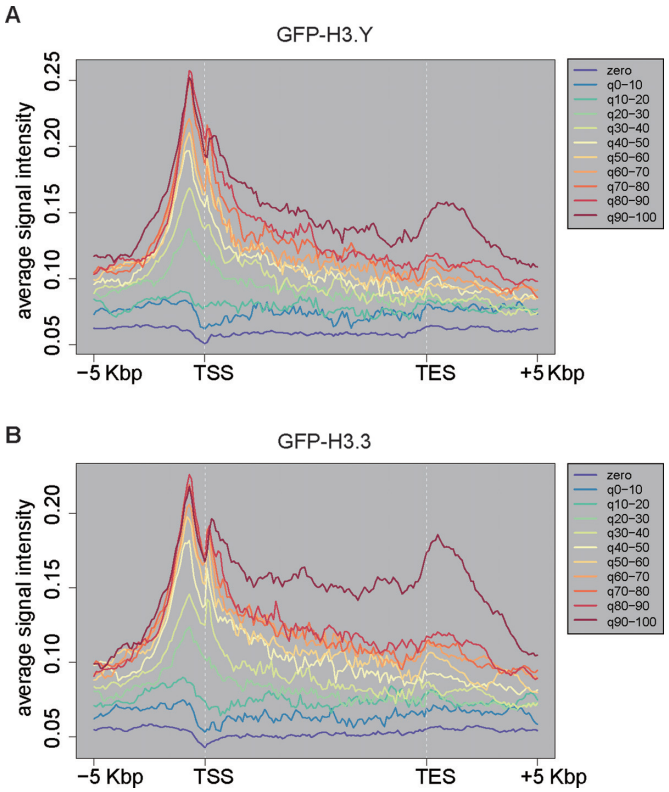

Figure 7. Genomic distribution of H3.Y. (**A** and **B**) Average genome-wide ChIP-seq signal intensities of (A) GFP-H3.Y and (B) H3.3 on genes in HeLa cells. The genes were classified into 11 groups, according to their mRNA levels (See Materials and Methods for details). The distribution of GFP-H3.Y or GFP-H3.3 was analyzed within the region 5 kbp upstream of the TSS to 5 kbp downstream of the TES.

sult suggests that GFP-H3.Y, as well as GFP-H3.3, was incorporated into nucleosomes by replacing the endogenous H3.

The mobility of GFP-H3.Y was then analyzed by FRAP. As shown in Figure 5C and D, the fluorescence recovery of GFP-H3.Y was as slow as that of GFP-H3.3, in good agreement with the results suggesting that the H3.Y was stably incorporated into the chromatin. The thermal stability assay (Figure 6A) revealed that the H3.Y-H4 tetramer associated with DNA more stably than the H3.3-H4 tetramer *in vitro* (Figure 6B). Surprisingly, we found that the H2A–H2B dimer dissociated more easily from the H3.Y nucleosome than the H3.3 nucleosome (Figure 6C). Therefore, the H3.Y nucleosome may have the tendency to release the H2A–H2B dimer more readily, although the H3.Y–H4 tetramer stably exists in chromatin.

H3.Y accumulates around transcription start sites in the human genome

We next assessed the genomic localization of the H3.Y nucleosome in human cells. In humans, H3.Y production is extremely limited, and is undetectable in HeLa cells (18). Therefore, we used the HeLa cells stably expressing GFP-H3.Y for chromatin immunoprecipitation experiments, although the production of GFP-H3.3 was about 2-fold higher than that of GFP-H3.Y in cells (Figure 5A). The genomic DNA fragments that co-precipitated with GFP-H3.Y were sequenced. We found that H3.Y was substantially enriched around the TSSs of actively transcribed genes (Figure 7A), as was H3.3 (Figure 7B). Maehara *et al.* reported that mouse H3.1, H3.2 and H3t are not specifically accumulated around TSSs, when they are exogenously produced in cells (62). Therefore, the accumulation of H3.Y at TSSs may not merely be due to the higher histone exchange around TSSs. The TSS enrichment of H3.Y, as well as H3.3, was reproduced in an independent set of experiments (Supplementary Figure S5). These results suggested that H3.Y may play a functional role around TSSs, and may regulate the transcription status of certain genes.

Reconstitution and characterization of the heterotypic nucleosome containing H3.Y and H3.3

A previous study suggested that H3.Y may form a heterotypic nucleosome, containing one each of H3.Y and H3.3 (18). Since the binding motif for the H3.3-specific chaperone, DAXX (63), is perfectly conserved between H3.Y and H3.3 (87-AAIG-90, Figure 1A), H3.Y and H3.3 may share the same histone chaperone. This suggested that H3.Y may be incorporated into the nucleosome together with H3.3, and predominantly form the H3.Y/H3.3 heterotypic nucleosome in cells.

To test whether the characteristics of the H3.Y nucleosome are conserved in the heterotypic H3.Y/H3.3 nucleosome, we reconstituted the heterotypic H3.Y/H3.3 nucleosome by the method established previously (29) (Supplementary Figure S6A and B). Histone H3.3 was prepared as a recombinant protein containing the His_6-SUMO tag at its N-terminus (His-SUMO-H3.3; Supplementary Figure S6C). The nucleosomes were reconstituted by the salt-dialysis method, with His-SUMO-H3.3 and untagged histones H2A, H2B and H4, resulting three types of H3 nucleosomes, the homotypic His-SUMO-H3.3 nucleosome, the homotypic H3.Y nucleosome and the heterotypic H3.Y/His-SUMO-H3.3 nucleosome. The heterotypic H3.Y/His-SUMO-H3.3 nucleosome migrated faster than the homotypic His-SUMO-H3.3 nucleosome, but slower than the homotypic H3.Y nucleosome. We then purified the H3.Y/His-SUMO-H3.3 nucleosome by preparative native PAGE (Supplementary Figure S6D). After the purification, the His_6-SUMO portion of the heterotypic H3.Y/His-SUMO-H3.3 nucleosome was proteolyzed by PreScission protease, and the resulting H3.Y/H3.3 nucleosome was further purified by a second round of preparative native PAGE (Supplementary Figure S6E and F).

The heterotypic H3.Y/H3.3 nucleosome was more susceptible to MNase than the H3.3 nucleosome (Figure 8A and B), indicating that the flexible nature of the DNA in the H3.Y nucleosome is also conserved. In addition, the H1 binding was also reduced in the heterotypic H3.Y/H3.3 nucleosome, as compared to the H3.3 nucleosome (Figure 8C and D). We therefore concluded that the H3.Y-specific characteristics are conserved in the heterotypic H3.Y/H3.3 nucleosome.

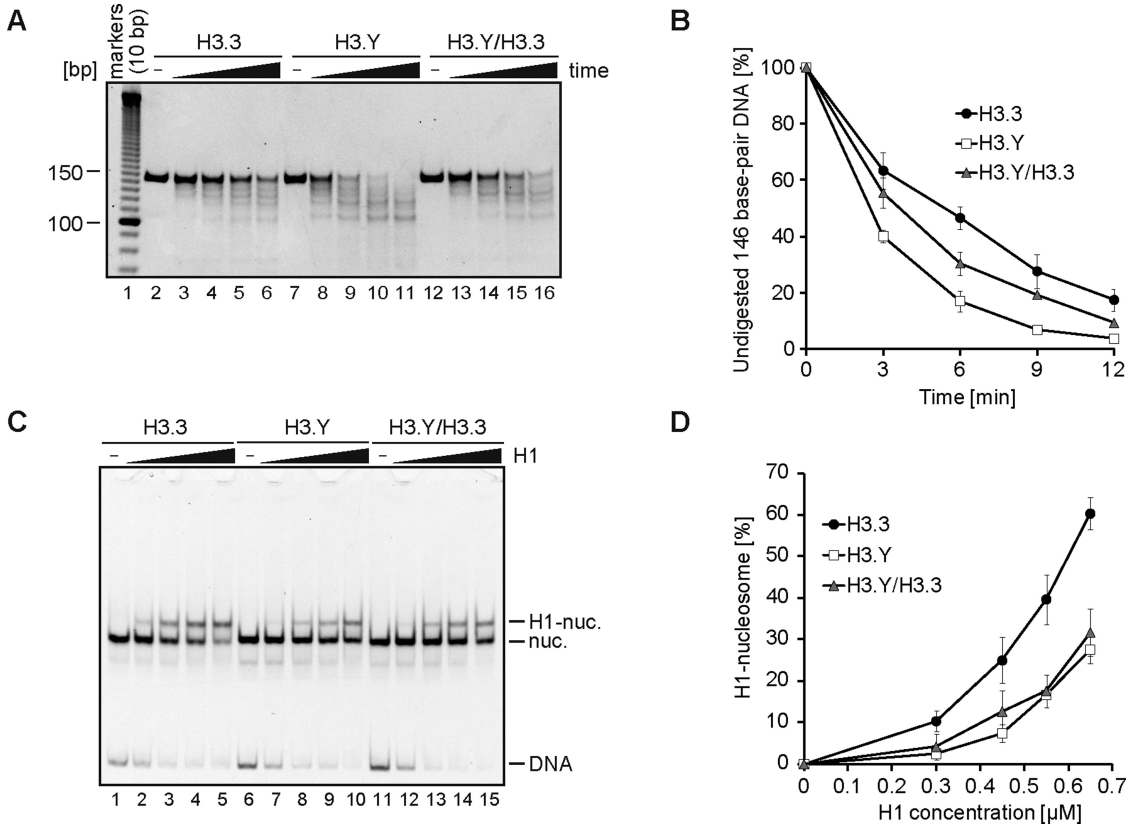

Figure 8. Biochemical analyses of the heterotypic H3.Y/H3.3 nucleosome. (**A**) MNase treatment assay. The H3.3 (lanes 2–6), H3.Y (lanes 7–11), and heterotypic H3.Y/H3.3 (lanes 12–16) nucleosomes containing a 146 base-pair DNA were incubated at 37°C for 0, 3, 6, 9 and 12 min, in the presence of MNase. After an incubation, the reaction was stopped with a proteinase K solution, containing EDTA and SDS, and the reaction products were analyzed by non-denaturing 6% PAGE with ethidium bromide staining. (**B**) Graphical representation of the MNase treatment assay. The band intensities of the remaining 146 base-pair DNA were quantitated, and the rate of undigested DNA [%] was plotted. The error bars indicate standard deviations (n = 3). (**C**) The H1 binding assay. Increasing amounts of H1 (0 μM: lanes 1, 6 and 11; 0.3 μM: lanes 2, 7 and 12; 0.45 μM: lanes 3, 7 and 13; 0.55 μM: lanes 4, 8 and 14; 0.65 μM: lanes 5, 9 and 15) were mixed with the H3.3 (lanes 1–5), H3.Y (lanes 6–10) and heterotypic H3.Y/H3.3 (lanes 11–15) nucleosomes (0.1 μM), in presence of Nap1 (0.3 μM). After an incubation at 37°C, the complexes were detected by non-denaturing 5% PAGE with ethidium bromide staining. (**D**) Graphical representation of the H1 binding assay. The band intensities corresponding to the H1-nucleosome complex and the nucleosomes were quantitated, and the rate of H1-nucleosome complex formation was plotted against the H1 concentration. The error bars indicate standard deviations (n = 3).

DISCUSSION

Histone H3.Y has been identified as a primate-specific histone variant. H3.Y mRNA expression is observed in primary cells from human testis and brain, except the thalamus, in addition to cancer cells, such as breast, lung, bone and ovary tumors (18). H3.Y production is also observed in the human osteosarcoma cell line, U2OS, especially under nutrient starvation and/or overgrowth conditions. The H3.Y knockdown significantly affects cell growth, and changes the expression profiles of many genes related to cell cycle control (18). However, the amount of the endogenous H3.Y protein is extremely low in these cells. These findings suggested that the H3.Y nucleosomes may be incorporated into specific genomic loci, and may regulate the genomic DNA function at these loci.

Previous analyses revealed that ectopically produced H3.Y preferentially localizes in transcriptionally active euchromatic regions, and many genes are supressed by H3.Y knockdown (18), implying that the H3.Y nucleosome actually plays a role in transcription activation. However, the mechanism by which the H3.Y nucleosome contributes to transcription activation has remained unknown, because no structural and biochemical studies have been reported.

To understand the contribution of H3.Y to chromatin structure and gene regulation, in the present study, we performed structural, biochemical and genomic analyses of human H3.Y. We obtained five major findings: (i) the H3.Y nucleosome forms a relaxed chromatin configuration (Figure 3), which is induced by its flexible DNA ends (Figure 2); (ii) the H3.Y nucleosome binds linker histone H1 less efficiently (Figure 4); (iii) the H3.Y nucleosome is very stable *in vitro* and *in vivo* (Figures 5 and 6); (iv) H3.Y preferentially accumulates on the transcription start sites of actively transcribed genes in cells (Figure 7); and (v) the DNA end flexibility and reduced H1 binding characteristics of the H3.Y nucleosome are conserved in the heterotypic H3.Y/H3.3 nucleosome (Figure 8), which may be the predominant form of the H3.Y-containing nucleosome in cells. It is interesting to imagine that the heterotypic H3.Y/H3.3 nucleosome may dictate the direction of transcription by its semi-flexible

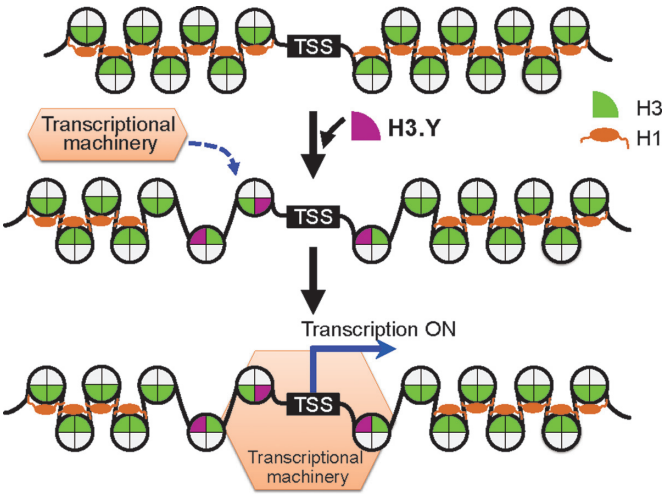

Figure 9. A model for the H3.Y nucleosome function. H3.Y (purple) predominantly accumulates around TSSs, probably forms the heterotypic H3.Y/H3.3 nucleosome, and reduces the binding of the linker histone H1 (second row). The resulting accessible chromatin region containing H3.Y may be targeted by the transcription machinery (third row). The stable properties of the H3.Y nucleosome enable it to stay around the TSS, and it maintains the relaxed chromatin configuration. This specific characteristic of the H3.Y nucleosome may allow it to continuously function during the transcription process, even the expression level of H3.Y is extremely low in cells.

nature. Future studies are awaited to understand these interesting questions.

Based on these findings and the previous reports, we propose a model for the regulation and function of H3.Y (Figure 9). H3.Y assembles into nucleosomes around TSSs, probably as the H3.Y/H3.3 heterotypic form. Once assembled, the H3.Y/H3.3 nucleosome is maintained and provides an accessible chromatin configuration platform, with flexible ends that reduce histone H1 binding. This is consistent with the previous genomic analysis, which revealed that H1 is generally depleted at active promoters (64). In such a relaxed chromatin configuration, the transcription enzymes, such as RNA polymerase, have better access to the TSS regions of active genes (Figure 9). Thus, the stable association of H3.Y in chromatin may function to maintain the active gene status. However, it is unclear how H3.Y becomes accumulated at TSSs. H3.Y shares the binding motif for the H3.3-specific chaperone, DAXX, with H3.3 (63, Figure 1A). If H3.Y employs the common assembly pathway with H3.3, then the TSS accumulation of H3.Y may be established as a result of the H3.Y removal from the gene body region, but not from TSSs. This may occur by nucleosome removal by a transcribing RNA polymerase.

The H3.Y-mediated relaxed chromatin formation is probably due to its DNA flexibility. DNA end flexibility has also been found in the nucleosome containing the centromeric H3 variant, CENP-A (52-55). However, the sedimentation assay revealed that the CENP-A poly-nucleosomes are rather compacted, as compared to the poly-nucleosomes containing H3 (54,65). Interestingly, Fang *et al.* showed that the compaction of the CENP-A poly-nucleosome strictly depends on the CENP-A specific RG loop (65). This loop is not conserved in other H3 variants, including H3.Y. Therefore, the compaction of the CENP-A poly-nucleosome may be mediated by a different mechanism from that of the H3.Y poly-nucleosome.

Finally, the stable chromatin association and TSS accumulation of H3.Y may underlie its function as an epigenetic marker, which allows the TSS location to be inherited in daughter cells. To do so, the cell-cycle dependent transition from the homotypic H3.Y/H3.Y nucleosome to the heterotypic H3.Y/H3.3 nucleosome may be required around TSSs. Identification of the H3.Y chaperone and/or exchange mechanism for the specific recruitment/displacement of H3.Y to promote this homotypic-heterotypic nucleosome transition is an important future issue to address.

ACCESSION NUMBERS

The structural data of the H3.Y nucleosome have been deposited to the Protein Data Bank (PDB ID: 5AY8). The mRNA-seq and ChIP-seq data have been deposited to DNA Data Bank of Japan (DDBJ, accession nos. DRA003923 for GFP-H3.Y and DRA002604 for GFP-H3.3).

SUPPLEMENTARY DATA

Supplementary Data are available at NAR Online.

ACKNOWLEDGEMENTS

We thank the beamline scientists for their assistance with data collection at the BL41XU beamline of SPring-8 and the BL-17A beamline of the Photon Factory. The synchrotron radiation experiments were performed with the approval of the Japan Synchrotron Radiation Research Institute (JASRI) [proposal nos. 2012A1125, 2012B1048, 2013A1036 and 2013B1060] and the Photon Factory Program Advisory Committee [proposal no. 2012G569].

FUNDING

MEXT KAKENHI [25116002 to H. Kurumizaka, 25116005 to H. Kimura and number 25116010 to Y.O., in part]; Platform Project for Supporting Drug Discovery and Life Science Research [Platform for Drug Discovery, Informatics, and Structural Life Science, partially]; Ministry of Education, Culture, Sports, Science and Technology (MEXT); Japan Agency for Medical Research and Development (AMED) (to H. Kurumizaka); Waseda Research Institute for Science and Engineering (to H. Kurumizaka and N.H.); Intramural programs of Waseda University (to H. Kurumizaka); Research Fellowships for Young Scientists from Japan Society for the Promotion of Science (T.K.). Funding for open access charge: Waseda University.
Conflict of interest statement. None declared.

REFERENCES

1. Wolffe,A. (1998) *Chromatin: Structure and Function*. 3rd edn. Academic Press, San Diego.
2. Luger,K., Mäder,A.W., Richmond,R.K., Sargent,D.F. and Richmond,T.J. (1997) Crystal structure of the nucleosome core particle at 2.8 Å resolution. *Nature*, **389**, 251–260.

3. Soboleva,T.A., Nekrasov,M., Ryan,D.P. and Tremethick,D.J. (2014) Histone variants at the transcription start-site. *Trends Genet.*, **30**, 199–209.
4. Venkatesh,S. and Workman,J.L. (2015) Histone exchange, chromatin structure and the regulation of transcription. *Nat. Rev. Mol. Cell. Biol.*, **16**, 178–189.
5. Strahl,B.D. and Allis,C.D. (2000) The language of covalent histone modifications. *Nature*, **403**, 41–45.
6. Berger,S. (2007) The complex language of chromatin regulation during transcription. *Nature*, **447**, 407–412.
7. Franklin,S.G. and Zweidler,A. (1977) Non-allelic variants of histones 2a, 2b and 3 in mammals. *Nature*, **266**, 273–275.
8. Palmer,D.K., O'Day,K., Wener,M.H., Andrews,B.S. and Margolis,R.L. (1987) A 17-kD centromere protein (CENP-A) copurifies with nucleosome core particles and with histones. *J. Cell Biol.*, **104**, 805–815.
9. Albig,W., Ebentheuer,J., Klobeck,G., Kunz,J. and Doenecke,D. (1996) A solitary human H3 histone gene on chromosome 1. *Hum. Genet.*, **97**, 486–491.
10. Witt,O., Albig,W. and Doenecke,D. (1996) Testis-specific expression of a novel human H3 histone gene. *Exp. Cell Res.*, **229**, 301–306.
11. Ahmad,K. and Henikoff,S. (2002) Histone H3 variants specify modes of chromatin assembly. *Proc. Natl. Acad. Sci. U.S.A.*, **99**(Suppl. 4), 16477–16484.
12. Malik,H.S. and Henikoff,S. (2003) Phylogenomics of the nucleosome. *Nat. Struct. Biol.*, **10**, 882–891.
13. Henikoff,S., McKittrick,E. and Ahmad,K. (2004) Epigenetics, histone H3 variants, and the inheritance of chromatin states. *Cold Spring Harb. Symp. Quant. Biol.*, **69**, 235–243.
14. Kamakaka,R.T. and Biggins,S. (2005) Histone variants: deviants? *Genes Dev.*, **19**, 295–310.
15. Hake,S.B. and Allis,C.D. (2006) Histone H3 variants and their potential role in indexing mammalian genomes: the "H3 barcode hypothesis". *Proc. Natl. Acad. Sci. U.S.A.*, **103**, 6428–6435.
16. Loyola,A. and Almouzni,G. (2007) Marking histone H3 variants: how, when and why? *Trends Biochem. Sci.*, **32**, 425–433.
17. Ray-Gallet,D. and Almouzni,G. (2010) Nucleosome dynamics and histone variants. *Essays Biochem.*, **48**, 75–87.
18. Wiedemann,S.M., Mildner,S.N., Bönisch,C., Israel,L., Maiser,A., Matheisl,S., Straub,T., Merkl,R., Leonhardt,H., Kremmer,E. *et al.* (2010) Identification and characterization of two novel primate-specific histone H3 variants, H3.X and H3.Y. *J. Cell Biol.*, **190**, 777–791.
19. Schenk,R., Jenke,A., Zilbauer,M., Wirth,S. and Postberg,J. (2011) H3.5 is a novel hominid-specific histone H3 variant that is specifically expressed in the seminiferous tubules of human testes. *Chromosoma*, **120**, 275–285.
20. Kaufman,P.D., Kobayashi,R., Kessler,N. and Stillman,B. (1995) The p150 and p60 subunits of chromatin assembly factor I: a molecular link between newly synthesized histones and DNA replication. *Cell*, **81**, 1105–1114.
21. Tagami,H., Ray-Gallet,D., Almouzni,G. and Nakatani,Y. (2004) Histone H3.1 and H3.3 complexes mediate nucleosome assembly pathways dependent or independent of DNA synthesis. *Cell*, **116**, 51–61.
22. Ray-Gallet,D., Quivy,J.P., Scamps,C., Martini,E.M., Lipinski,M. and Almouzni,G. (2002) HIRA is critical for a nucleosome assembly pathway independent of DNA synthesis. *Mol. Cell*, **9**, 1091–1100.
23. Elsaesser,S.J., Goldberg,A.D. and Allis,C.D. (2010) New functions for an old variant: no substitute for histone H3.3. *Curr. Opin. Genet. Dev.*, **20**, 110–117.
24. Drané,P., Ouararhni,K., Depaux,A., Shuaib,M. and Hamiche,A. (2010) The death-associated protein DAXX is a novel histone chaperone involved in the replication-independent deposition of H3.3. *Genes Dev.*, **24**, 1253–1265.
25. Goldberg,A.D., Banaszynski,L.A., Noh,K.M., Lewis,P.W., Elsaesser,S.J., Stadler,S., Dewell,S., Law,M., Guo,X., Li,X. *et al.* (2010) Distinct factors control histone variant H3.3 localization at specific genomic regions. *Cell*, **140**, 678–691.
26. Szenker,E., Ray-Gallet,D. and Almouzni,G. (2011) The double face of the histone variant H3.3. *Cell Res.*, **21**, 421–434.
27. Tanaka,Y., Tawaramoto-Sasanuma,M., Kawaguchi,S., Ohta,T., Yoda,K., Kurumizaka,H. and Yokoyama,S. (2004) Expression and purification of recombinant human histones. *Methods*, **33**, 3–11.
28. Tachiwana,H., Osakabe,A., Shiga,T., Miya,Y., Kimura,H., Kagawa,W. and Kurumizaka,H. (2011) Structures of human nucleosomes containing major histone H3 variants. *Acta Crystallogr. D Biol. Crystallogr.*, **67**, 578–583.
29. Arimura,Y., Shirayama,K., Horikoshi,N., Fujita,R., Taguchi,H., Kagawa,W., Fukagawa,T., Almouzni,G. and Kurumizaka,H. (2014) Crystal structure and stable property of the cancer-associated heterotypic nucleosome containing CENP-A and H3.3. *Sci. Rep.*, **4**, 7115.
30. Tachiwana,H., Osakabe,A., Kimura,H. and Kurumizaka,H. (2008) Nucleosome formation with the testis-specific histone H3 variant, H3t, by human nucleosome assembly proteins in vitro. *Nucleic Acids Res.*, **36**, 2208–2218.
31. Machida,S., Takaku,M., Ikura,M., Sun,J., Suzuki,H., Kobayashi,W., Kinomura,A., Osakabe,A., Tachiwana,H., Horikoshi,Y. *et al.* (2014) Nap1 stimulates homologous recombination by RAD51 and RAD54 in higher-ordered chromatin containing histone H1. *Sci. Rep.*, **4**, 4863.
32. Lowary,P.T. and Widom,J. (1998) New DNA sequence rules for high affinity binding to histone octamer and sequence-directed nucleosome positioning. *J. Mol. Biol.*, **276**, 19–42.
33. Dyer,P.N., Edayathumangalam,R.S., White,C.L., Bao,Y., Chakravarthy,S., Muthurajan,U.M. and Luger,K. (2004) Reconstitution of nucleosome core particles from recombinant histones and DNA. *Methods Enzymol.*, **375**, 23–44.
34. Arimura,Y., Tachiwana,H., Oda,T., Sato,M. and Kurumizaka,H. (2012) Structural analysis of the hexasome, lacking one histone H2A/H2B dimer from the conventional nucleosome. *Biochemistry*, **51**, 3302–3309.
35. Tachiwana,H., Kagawa,W., Osakabe,A., Kawaguchi,K., Shiga,T., Hayashi-Takanaka,Y., Kimura,H. and Kurumizaka,H. (2010) Structural basis of instability of the nucleosome containing a testis-specific histone variant, human H3T. *Proc. Natl. Acad. Sci. U.S.A.*, **107**, 10454–10459.
36. Otwinowski,Z. and Minor,W. (1997) Processing of X-ray diffraction data collected in oscillation mode. *Methods Enzymol.*, **276**, 307–326.
37. McCoy,A.J., Grosse-Kunstleve,R.W., Adams,P.D., Winn,M.D., Storoni,L.C. and Read,R.J. (2007) Phaser crystallographic software. *J. Appl. Crystallogr.*, **40**, 658–674.
38. Adams,P.D., Afonine,P.V., Bunkóczi,G., Chen,V.B., Davis,I.W., Echols,N., Headd,J.J., Hung,L.W., Kapral,G.J., Grosse-Kunstleve,R.W. *et al.* (2010) PHENIX: a comprehensive Python-based system for macromolecular structure solution. *Acta Crystallogr. D Biol. Crystallogr.*, **66**, 213–221.
39. Emsley,P. and Cowtan,K. (2004) Coot: model-building tools for molecular graphics. *Acta Crystallogr. D Biol. Crystallogr.*, **60**, 2126–2132.
40. Chen,V.B., Arendall,W.B. 3rd, Headd,J.J., Keedy,D.A., Immormino,R.M., Kapral,G.J., Murray,L.W., Richardson,J.S. and Richardson,D.C. (2010) MolProbity: all-atom structure validation for macromolecular crystallography. *Acta Crystallogr. D Biol. Crystallogr.*, **66**, 12–21.
41. Syed,S.H., Goutte-Gattat,D., Becker,N., Meyer,S., Shukla,M.S., Hayes,J.J., Everaers,R., Angelov,D., Bednar,J. and Dimitrov,S. (2010) Single-base resolution mapping of H1-nucleosome interactions and 3D organization of the nucleosome. *Proc. Natl. Acad. Sci. U.S.A.*, **107**, 9620–9625.
42. Ranjan,A., Wang,F., Mizuguchi,G., Wei,D., Huang,Y. and Wu,C. (2015) H2A histone-fold and DNA elements in nucleosome activate SWR1-mediated H2A.Z replacement in budding yeast. *Elife*, **4**, e06845.
43. Taguchi,H., Horikoshi,N., Arimura,Y. and Kurumizaka,H. (2014). A method for evaluating nucleosome stability with a protein-binding fluorescent dye. *Methods*, **70**, 119–126.
44. Dorigo,B., Schalch,T., Bystricky,K. and Richmond,T.J. (2003) Chromatin fiber folding: requirement for the histone H4 N-terminal tail. *J. Mol. Biol.*, **327**, 85–96.
45. Demeler,B. and van Holde,K.E. (2004) Sedimentation velocity analysis of highly heterogeneous systems. *Anal. Biochem.*, **335**, 279–288.
46. Kimura,H., Takizawa,N., Allemand,E., Hori,T., Iborra,F.J., Nozaki,N., Muraki,M., Hagiwara,M., Krainer,A.R., Fukagawa,T. *et al.* (2006) A novel histone exchange factor, protein phosphatase 2Cgamma, mediates the exchange and dephosphorylation of H2A-H2B. *J. Cell Biol.*, **175**, 389–400.

47. Trapnell,C., Roberts,A., Goff,L., Pertea,G., Kim,D., Kelley,D.R., Pimentel,H., Salzberg,S.L., Rinn,J.L. and Pachter,L. (2012) Differential gene and transcript expression analysis of RNA-seq experiments with TopHat and Cufflinks. *Nat. Protoc.*, **7**, 562–578.
48. Harada,A., Okada,S., Konno,D., Odawara,J., Yoshimi,T., Yoshimura,S., Kumamaru,H., Saiwai,H., Tsubota,T., Kurumizaka,H. *et al.* (2012) Chd2 interacts with H3.3 to determine myogenic cell fate. *EMBO J.*, **31**, 2994–3007.
49. Mortazavi,A., Williams,B.A., McCue,K., Schaeffer,L. and Wold,B. (2008) Mapping and quantifying mammalian transcriptomes by RNA-Seq. *Nat. Methods*, **5**, 621–628.
50. Zhang,Y., Liu,T., Meyer,C.A., Eeckhoute,J., Johnson,D.S., Bernstein,B.E., Nusbaum,C., Myers,R.M., Brown,M., Li,W. *et al.* (2008) Model-based analysis of ChIP-Seq (MACS). *Genome Biol.*, **9**, R137.
51. Davey,C.A., Sargent,D.F., Luger,K., Maeder,A.W. and Richmond,T.J. (2002). Solvent mediated interactions in the structure of the nucleosome core particle at 1.9 Å resolution. *J. Mol. Biol.*, **319**, 1097–1113.
52. Conde e Silva,N., Black,B.E., Sivolob,A., Filipski,J., Cleveland,D.W. and Prunell,A. (2007) CENP-A-containing nucleosomes: easier disassembly versus exclusive centromeric localization. *J. Mol. Biol.*, **370**, 555–573.
53. Tachiwana,H., Kagawa,W., Shiga,T., Osakabe,A., Miya,Y., Saito,K., Hayashi-Takanaka,Y., Oda,T., Sato,M., Park,S.Y. *et al.* (2011). Crystal structure of the human centromeric nucleosome containing CENP-A. *Nature*, **476**, 232–235.
54. Panchenko,T., Sorensen,T. C., Woodcock,C.L., Kan,Z.Y., Wood,S., Resch,M.G., Luger,K., Englander,S.W., Hansen,J.C. and Black,B.E. (2011). Replacement of histone H3 with CENP-A directs global nucleosome array condensation and loosening of nucleosome superhelical termini. *Proc. Natl. Acad. Sci. U.S.A.*, **108**, 16588–16593.
55. Dechassa,M.L., Wyns,K., Li,M., Hall,M.A., Wang,M.D. and Luger,K. (2011). Structure and Scm3-mediated assembly of budding yeast centromeric nucleosomes. *Nat. Commun.*, **2**, 313.
56. Hansen,J.C. and Lohr,D. (1993) Assembly and structural properties of subsaturated chromatin arrays. *J. Biol. Chem.*, **268**, 5840–5848.
57. Fan,J.Y., Gordon,F., Luger,K., Hansen,J.C. and Tremethick,D.J. (2002) The essential histone variant H2A.Z regulates the equilibrium between different chromatin conformational states. *Nat. Struct. Biol.*, **9**, 172–176.
58. Schwarz,P.M. and Hansen,J.C. (1994) Formation and stability of higher order chromatin structures. Contributions of the histone octamer. *J. Biol. Chem.*, **269**, 16284–16289.
59. Schwarz,P.M., Felthauser,A., Fletcher,T.M. and Hansen,J.C. (1996) Reversible oligonucleosome self-association: dependence on divalent cations and core histone tail domains. *Biochemistry*, **35**, 4009–4015.
60. Saeki,H., Ohsumi,K., Aihara,H., Ito,T., Hirose,S., Ura,K. and Kaneda,Y. (2005) Linker histone variants control chromatin dynamics during early embryogenesis. *Proc. Natl. Acad. Sci. U.S.A.*, **102**, 5697–5702.
61. Shintomi,K., Iwabuchi,M., Saeki,H., Ura,K., Kishimoto,T. and Ohsumi,K. (2005) Nucleosome assembly protein-1 is a linker histone chaperone in Xenopus eggs. *Proc. Natl. Acad. Sci. U.S.A.*, **102**, 8210–8215.
62. Maehara,K., Harada,A., Sato,Y., Matsumoto,M., Nakayama,K. I., Kimura,H. and Ohkawa,Y. (2015). Tissue-specific expression of histone H3 variants diversified after species separation. *Epigenet. Chromatin*, **8**, 1–17.
63. Elsaesser,S.J., Huang,H., Lewis,P.W., Chin,J.W., Allis,C.D. and Patel,D.J. (2012) DAXX envelops a histone H3.3-H4 dimer for H3.3-specific recognition. *Nature*, **491**, 560–565.
64. Izzo,A., Kamieniarz-Gdula,K., Ramírez,F., Noureen,N., Kind,J., Manke,T., van Steensel,B. and Schneider,R. (2013) The genomic landscape of the somatic linker histone subtypes H1.1 to H1.5 in human cells. *Cell Rep.*, **3**, 2142–2154.
65. Fang,J., Liu,Y., Wei,Y., Deng,W., Yu,Z., Huang,L., Teng,Y., Yao,T., You,Q., Ruan,H. *et al.* (2015). Structural transitions of centromeric chromatin regulate the cell cycle-dependent recruitment of CENP-N. *Genes Dev.*, **29**, 1058–1073.